

## FUNDAMENTAL VIBRATIONAL TRANSITION OF CO DURING THE OUTBURST OF EX LUPU IN 2008<sup>1,2</sup>

M. GOTO,<sup>3</sup> Zs. REGÁLY<sup>4</sup>, C. P. DULLEMOND<sup>3</sup>, M. VAN DEN ANCKER<sup>5</sup>, J. M. BROWN<sup>6</sup>, A. CARMONA<sup>7</sup>, K. PONTOPPIDAN<sup>8</sup>,  
P. ÁBRAHÁM<sup>4</sup>, G. A. BLAKE<sup>8</sup>, D. FEDELE<sup>3,9</sup>, TH. HENNING<sup>3</sup>, A. JUHÁSZ<sup>3</sup>, Á. KÓSPÁL<sup>10</sup>, L. MOSONI<sup>3,4</sup>, A.  
SICILIA-AGUILAR<sup>3</sup>, H. TERADA<sup>11</sup>, R. VAN BOEKEL<sup>3</sup>, E. F. VAN DISHOECK<sup>8,10</sup>, T. USUDA<sup>11</sup>

*Draft version June 2, 2021*

### ABSTRACT

We report monitoring observations of the T Tauri star EX Lupi during its outburst in 2008 in the CO fundamental band at 4.6–5.0  $\mu\text{m}$ . The observations were carried out at the *VLT* and the Subaru Telescope at six epochs from April to August 2008, covering the plateau of the outburst and the fading phase to a quiescent state. The line flux of CO emission declines with the visual brightness of the star and the continuum flux at 5  $\mu\text{m}$ , but composed of two subcomponents that decay with different rates. The narrow line emission (50  $\text{km s}^{-1}$  in FWHM) is near the systemic velocity of EX Lupi. These emission lines appear exclusively in  $v=1-0$ . The line widths translate to a characteristic orbiting radius of 0.4 AU. The broad line component (FWZI  $\sim 150 \text{ km s}^{-1}$ ) is highly excited upto  $v \leq 6$ . The line flux of the component decreases faster than the narrow line emission. Simple modeling of the line profiles implies that the broad-line emitting gas is orbiting around the star at 0.04–0.4 AU. The excitation state, the decay speed of the line flux, and the line profile, indicate that the broad-line emission component is physically distinct from the narrow-line emission component, and more tightly related to the outburst event.

*Subject headings:* circumstellar matter — planetary systems: protoplanetary disks — stars: activity: other — stars: pre-main sequence — stars: formation — stars: individual (EX Lupi)

### 1. INTRODUCTION

EX Lupi, the prototype of the class of the eruptive pre-main sequence stars called EXors,<sup>12</sup> underwent its largest outburst recorded in the past 50 years in early 2008 (history of the observations of EX Lupi and EXors: Herbig 2007, 2008). The observational definition of EXor variables relies strongly on the prototype EX Lupi, which spectroscopically looks like a classical T Tauri star in the quiescent phase (Herbig 1950, 2001), but flares

by 1–3 magnitudes in the visible roughly once a decade, with each outbreak lasting about a year (Herbig 2007). The spectroscopic behavior in the outburst is complicated, and sometimes related to an expanding stellar shell (e.g. Herbig 1989). It is increasingly accepted, however, that the circumstellar disk plays the primary role in the outbursts, in which mass accreted from the envelope is stalled somewhere in the disk, until it reaches a critical surface density and triggers a disk instability.

The idea that EXor outbursts arise inside the accretion disk originates in their observational similarity with FUors. The most compelling evidence that the FUor outburst has its origin in a disk is the split absorption lines in the visible to the near-infrared with wavelength separation of two absorption peaks gradually decreasing with the wavelength (Hartmann, Hinkle, & Calvet 2004). This is most naturally accounted for when the absorption lines at long wavelengths arise from the cool outer part of the disk, where the orbital velocity is slower (e.g. Zhu et al. 2009). FUors and EXors are historically considered as different classes of eruptive pre-main sequence stars. However, both classes may represent a similar eruptive event, and differ only quantitatively in terms of flare amplitude, outburst duration, and outburst frequency. Recent outbursts of V1647 Ori (the central source of “McNeal’s Nebula”, e.g. Aspin, Beck, & Reipurth 2008) are recurrent like EXors, yet the amplitude of the outburst is more compatible with FUors, which fills the gap between these two classes. The mass accreted in a single outburst and the frequency of the outbursts indicates that an EXor/FUor star acquires a substantial fraction of its mass solely during the outbursts. It lends circumstantial support to the theory that EXors/FUors are not a group of special variable stars, but a state of the accretion phase

mgoto@mpia.de

<sup>1</sup> Based on data collected in the course of CRIRES Large program [179.C-0151] and DDT program [281.C-4031(D,E,F)] at the *VLT* on Cerro Paranal (Chile), which is operated by the European Southern Observatory (ESO).

<sup>2</sup> Based on data collected at Subaru Telescope, which is operated by the National Astronomical Observatory of Japan.

<sup>3</sup> Max-Planck-Institut für Astronomie, Königstuhl 17, D-69117 Heidelberg, Germany.

<sup>4</sup> Konkoly Observatory, Konkoly Thege Miklós 15-17, H-1121 Budapest, Hungary.

<sup>5</sup> ESO, Karl-Schwarzschild-Straße 2, D-85748 Garching bei München, Germany.

<sup>6</sup> Max-Planck-Institut für extraterrestrische Physik, Giessenbachstraße D-85748 Garching bei München, Germany.

<sup>7</sup> ISDC Data Centre for Astrophysics & Geneva Observatory, University of Geneva, chemin d’Ecogia 16, 1290 Versoix, Switzerland.

<sup>8</sup> California Institute of Technology Division of Geological & Planetary Sciences, MC 170-25 1200 E. California Blvd., Pasadena, CA 91125, USA.

<sup>9</sup> Johns Hopkins University, Department of Physics and Astronomy 3701 San Martin drive Baltimore, MD 21218 USA.

<sup>10</sup> Leiden Observatory, Leiden University, P.O. Box 9513 NL-2300 RA Leiden, The Netherlands.

<sup>11</sup> Subaru Telescope, 650 North A’ohoku Place, Hilo, HI 96720, USA.

<sup>12</sup> The group of low-mass stars with large variability is coined as EXors by Herbig (1989) for its nature of the outburst similar to FU Ori variables that are collectively called FUors.

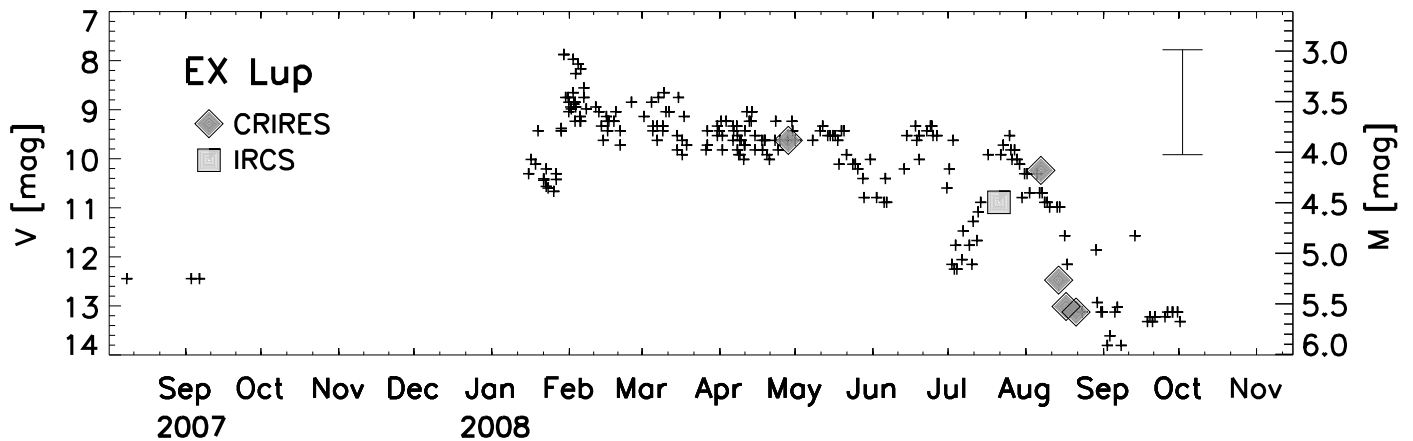


FIG. 1.— Light curve in the visible (crosses; from AAVSO <http://www.aavso.org/>) with the ordinate to the left, and in  $M$  band (diamonds for CRIREs, and a square for IRCS) to the right. The axis of  $M$  band magnitude is arbitrarily scaled to that of  $V$  band. The  $M$  band photometry is performed with the spectroscopic data, with the continuum level of the spectroscopic standard star as the photometric reference. The uncertainty of  $M$  band photometry is  $\pm 0.5$  mag (the error bar shown in the upper right corner).

that stars commonly experience during their evolution (e.g. Hartmann & Kenyon 1996). However, there are indeed qualitative differences between FUors and normal T Tauri stars, such as the clustering nature, as FUors tend to be in isolation, while other T Tauri stars are in clusters (Herbig, Petrov, & Duemmler 2003). Moreover, the number of known FUors in the Orion Nebula Cluster falls short if all class I sources go through the FUor phase with a finite duty cycle (Fedele et al. 2007), although the number may increase with the inclusion of the “FUor-like” stars being identified recently (Greene, Aspin, & Reipurth 2008). The current focus of EXor studies is to understand (1) what is the mechanism of the disk instability, (2) what is the relationship between EXors and FUors, and (3) what is the role of EXor/FUor events in the context of star formation.

In this report, we will concentrate on the cause of the disk instability and the physical scale of the outburst, as it often gives a clue to the trigger of the instability. The most favored model to date, thermal instability in a disk, is induced by ionization, and subsequent opacity increase due to negative hydrogen ions (Bell, Lin & Ruden 1991; Clarke et al. 1989). The thermal instability is therefore only operational within a limited disk radius, where atomic hydrogen is subject to thermal ionization. If the physical size of the outburst is larger, magnetohydrodynamic (MHD) instability may be favored, as it predicts a massive accretion in the magnetic dead zone at 1–10 AU (Armitage et al. 2001). If the outburst involves the whole disk, the scenario of an unseen companions leading to global disk instability may also work (Bonnell & Bastien 1992).

The vibrational transitions of CO are a unique probe of the inner regions of disks (0.01–1 AU) due to their high critical density ( $n_{\text{cr}} > 10^{10} \text{ cm}^{-3}$ ) and high excitation energy ( $\Delta E_{v=1-0} > 3000 \text{ K}$ ). Measurement of the location of the emitting gas is relatively straightforward under the assumption that the gas is in Keplerian rotation (e.g. Najita et al. 1996). We utilized multi-epoch observations of CO vibrational transitions in EX Lupi to constrain where in the disk the hot gas is located during the outburst, and how its physical property develops with time. The present study is part of the first multi-wavelength campaign of EX Lupi from the optical

(Sicilia-Aguilar et al. 2010), near-infrared (Kóspál et al. 2010) to mid-infrared wavelengths (Ábrahám et al. 2009; Juhász et al. 2010) during the 2008 eruption. We will use  $d = 155 \text{ pc}$  as the distance to EX Lupi from Lombardi et al. (2008), and the stellar parameters from Gras-Velázquez & Ray (2005) following Sipos et al. (2009) (Table 1).

## 2. OBSERVATIONS

The spectroscopic observations of the CO fundamental band were performed at the *VLT* and the Subaru Telescope over a total of 6 epochs (Figure 1). Half of the data were obtained in the director’s discretionary time (DDT) on 14, 17, and 21 August 2008 at the *VLT*. Two wavelength intervals of the CO fundamental band (4.66–4.77  $\mu\text{m}$  and 4.86–4.99  $\mu\text{m}$  with gaps between the four detector chips) were observed with CRIREs (Käufl et al. 2004) to cover the low [ $P(1)$ – $P(11)$ ] and the high [ $P(21)$ – $P(32)$ ] rotational transitions of  $v=1-0$  in order to provide good constraints on the rotational excitation temperature of the hot gas. The slit width was  $0''.2$ , corresponding to a nominal spectral resolution of  $R=100,000$  ( $\Delta v=3 \text{ km s}^{-1}$ ). The spectra were recorded by nodding the telescope along the slit to remove the sky background. The slit was oriented along P.A. =  $0^\circ$ ,  $180^\circ$ ,  $90^\circ$  and  $270^\circ$  by rotating the image rotator for the possible use of the data for spectroastrometry. Unfortunately, the achieved signal to noise ratio was not sufficient to extract any meaningful astrometric signal. The data obtained with different P.A. were simply summed and reduced as classical spectroscopic data. The total integration time was 12 and 16 minute for each grating setting. The MACAO adaptive optics system (Bonnet et al. 2004) was used with EX Lupi itself as the guide star. Spectroscopic standard stars were observed at close airmass with a same instrument setup.

EX Lupi was also observed by CRIREs at the *VLT* in the framework of the ESO large program 179.C-0151 on April 28 and August 7 in 2008. The observations covered the CO spectrum at 4.65–4.77  $\mu\text{m}$  with additional coverage at 4.81–4.90  $\mu\text{m}$  in the August observations. The slit width and the AO settings were the same as during the DDT observations. The total exposure times were about 20 min per grating setting in both of the nights.

TABLE 1  
STELLAR PARAMETERS FOR EX LUP1  
USED IN THIS PAPER.

		Reference
$M_*$ ...	$0.6 M_\odot$	1.
$R_*$ ...	$1.6 R_\odot$	1.
$L_*$ ...	$0.5 L_\odot$	1.
$d^a$ ...	155 pc	2.
$v_{\text{LSR}}^b$ ...	$\approx 0 \text{ km s}^{-1}$	3.

NOTE. — Reference: 1. Gras-Velázquez & Ray (2005), 2. Lombardi et al. (2008), 3. Herbig, Petrov, & Duemmler (2003).

<sup>a</sup> Distance to EX Lupi.

<sup>b</sup> Systemic velocity as measured with optical spectroscopy.

IRCS (Tokunaga et al. 1998) at the Subaru Telescope was used to obtain CO fundamental band spectra of EX Lupi on 21 July 2008. The angle of the echelle grating was set so that the spectral interval of 4.65–4.74  $\mu\text{m}$  was covered by the detector. The  $0''.15$  slit was used resulting in a spectral resolution of  $R=20,000$  ( $\Delta v = 15 \text{ km s}^{-1}$ ). The spectra were recorded by nodding the tip-tilt mirror inside the AO system  $3''.4$  along the slit to remove the sky background. The observation was performed through a large airmass ( $\sec z \sim 2$ ) with 5 times lower spectral resolution than CRIRES. Thus, the data quality is significantly lower. The total integration time was 14 minutes. The adaptive optics system (Hayano et al. 2008) was also used here with EX Lupi as the guide star. The observations of all 6 epochs are summarized in Table 2.

One-dimensional spectra were extracted from the CRIRES dataset using the `crires_spec_jitter` recipe<sup>13</sup> on the ESO gasgano platform<sup>14</sup>. A custom-written IDL code was used to divide the spectra of EX Lupi by standard star spectra to eliminate telluric absorption lines. In the cases where the precipitable water vapor varied during the night, the water absorption was removed from both the object and the standard spectra beforehand by dividing them by the ATRAN atmospheric transmission model (Lord 1992). The IDL code further corrected wavelength offsets between EX Lupi and the spectroscopic standard spectra, slight differences in spectral resolution, and mismatches of the airmass. The wavelength calibration was performed by maximizing the cross-correlation between the observed spectra and the atmospheric transmission curve. The wavelength calibration error depends on the density of the telluric lines, and is less than a few pixels ( $\sim 5 \text{ km s}^{-1}$ ).

The IRCS data were reduced in the same way, except that the IRAF<sup>15</sup> aperture extraction package was used to extract the one-dimensional spectra.

EX Lupi is an M0 star in its quiescent phase with CO bandhead absorption at 2.3  $\mu\text{m}$  (Sipos et al. 2009).

Nevertheless, the photospheric correction for the CO absorption lines was not performed at 4.7  $\mu\text{m}$ , as the photospheric temperature during the outburst is unknown. The contribution of the stellar photosphere at 5  $\mu\text{m}$  is less than 20% in the quiescent phase (Sipos et al. 2009), and expected to be less during the outburst (Juhász et al. 2010).

Since there is no simultaneous photometry available at 5  $\mu\text{m}$ , the absolute flux calibration was performed against the spectroscopic standard stars HR 6084, HR 5987, and HR 6508. HR 6084 is a B1 III star with an  $M$  band magnitude of 2.42 mag<sup>16</sup>. HR 5987 and HR 6508 are B2.5 Vn and B2 IV stars with  $K$  magnitudes of 4.70 and 3.18 mag, respectively, but without accurate  $M$  band brightness documented. We applied a color correction of  $K - M = -0.05$  mag taken from  $K - L$  of early B stars [Tokunaga (1999) with the original from Koornneef (1983)], that gives  $M = 4.75$  and 3.23 mag, respectively. The precise correction is unimportant, since the overall photometric accuracy is only  $\pm 0.5$  mag. The main source of photometric error is the variable slit transmission at the time of the observation up to a factor of three even in a pair of consecutive frames. The variable atmospheric transmission during the nights adds another 30% to the photometric uncertainty. EX Lupi becomes fainter from 3.9 to 5.6 mag in the  $M$  band over 4 months (Table 2). The photometric value on 28 April is surprisingly bright, as Spitzer spectroscopy in April 2008 indicates 1.5 Jy at 5  $\mu\text{m}$ , or  $M \approx 5.0$  mag (Juhász et al. 2010). Since then, the star became fainter at optical wavelengths<sup>17</sup>, albeit with significant variability on timescales of days to weeks. The data counts in the raw frames are at least consistent with those of  $M=3.9$ –5.6 mag stars, as simulated by the exposure time calculator of CRIRES<sup>18</sup>.

### 3. ANALYSIS

#### 3.1. Two Emission Components

All spectra from the 6 epochs are shown in Fig. 2 after having been normalized to the continuum and corrected to the local standard of the rest. Two spectral components are immediately noticeable in the CO spectra, one broad [full width at zero intensity (FWZI)  $\sim 150 \text{ km s}^{-1}$ ] and one narrow [full width at half maximum (FWHM)  $\sim 50 \text{ km s}^{-1}$ ] overlaid on each other. The broad line emission is characterized by the hot vibrational transitions up to  $v=6$  confirmed. This is in agreement with the first overtone band in emission seen at least up to  $v=5-3$  in the SINFONI spectra (Kóspál et al. 2010) observed on 25–31 July prior to the CRIRES DDT runs during the outburst. In order to illustrate the broad line profiles of the former, a few lines from  $v \geq 2$  levels, which are relatively isolated from others, such as  $P(3) v=2-1$  at 4.750  $\mu\text{m}$  and  $R(9) v=3-2$  at 4.703  $\mu\text{m}$ , are combined and shown in the left panel of Fig. 3. The broad emission lines are most clearly seen in the April 28 data, taken during the outburst, a few months after the optical maximum.

The sharp emission lines on top of the broad component are close to the systemic velocity of EX Lupi

<sup>13</sup> CRIRES Pipeline User Manual VLT-MAN-ESO-19500-4406.

<sup>14</sup> <http://www.eso.org/sci/data-processing/software/gasgano/>.

<sup>15</sup> IRAF is distributed by the National Optical Astronomy Observatories, which are operated by the Association of Universities for Research in Astronomy, Inc., under cooperative agreement with the National Science Foundation.

<sup>16</sup> [http://www.jach.hawaii.edu/UKIRT/astronomy/calib/photocal/bright\\_std.html](http://www.jach.hawaii.edu/UKIRT/astronomy/calib/photocal/bright_std.html)

<sup>17</sup> AAVSO <http://www.aavso.org/>.

<sup>18</sup> <http://www.eso.org/observing/etc/>.

TABLE 2  
JOURNAL OF OBSERVATION.

Epoch	Program	JD	$V$ [mag] <sup>a</sup>	$M$ [mag] <sup>b</sup>	Spectrograph	Telescope	Velocity Resolution	Wavelength Coverage	Integration Time [min] <sup>c</sup>	Standard Star	Spectral Type
28 Apr 2008	179.C-0151(D)	2454585	9.7	3.88	CRIRES	VLT	3 km s <sup>-1</sup>	4.65–4.77 $\mu\text{m}$	20	HR 6084	B1 III
21 Jul 2008	DDT	2454669	10.0	4.50	IRCS	Subaru	15 km s <sup>-1</sup>	4.65–4.74 $\mu\text{m}$	14	HR 5987	B2.5Vn
7 Aug 2008	179.C-0151(D)	2454686	10.8	4.18	CRIRES	VLT	3 km s <sup>-1</sup>	4.65–4.77 $\mu\text{m}$ , 4.80–4.90 $\mu\text{m}$	20	HR 6084	B1 III
14 Aug 2008	281.C-4031(D)	2454693	11.1	5.27	CRIRES	VLT	3 km s <sup>-1</sup>	4.66–4.77 $\mu\text{m}$ <sup>d</sup> 4.86–4.99 $\mu\text{m}$ <sup>d</sup>	12, 16	HR 6508	B2IV
17 Aug 2008	281.C-4031(E)	2454696	12.3	5.53	CRIRES	VLT	3 km s <sup>-1</sup>	4.66–4.77 $\mu\text{m}$ <sup>d</sup> 4.86–4.99 $\mu\text{m}$ <sup>d</sup>	12, 16	HR 6508	B2IV
21 Aug 2008	281.C-4031(F)	2454700	13.3	5.58	CRIRES	VLT	3 km s <sup>-1</sup>	4.66–4.77 $\mu\text{m}$ <sup>d</sup> 4.86–4.99 $\mu\text{m}$ <sup>d</sup>	12, 16	HR 6508	B2IV

<sup>a</sup> From AAVSO <http://www.aavso.org/>.

<sup>b</sup> Photometry is done with respect to the spectroscopic standard stars. The accuracy is  $\pm 0.5$  mag.

<sup>c</sup> For one grating setting.

<sup>d</sup> With gaps between the four detector chips.

( $v_{\text{LSR}} \approx 0$  km s<sup>-1</sup>; Herbig, Petrov, & Duemmler 2003). The intensity of the narrow lines is 10–20% above the continuum level throughout the observations. The line profile of the emission lines does not change significantly during and at the end of the outburst (Fig. 3, right). The line widths, markedly smaller than the broad line component, imply that the emission arises from regions of the disk outside where the broad and highly-excited emission lines comes from.

The spectral profile, composed of two distinct kinematic components, is somewhat similar to Fe II at 5018 Å observed with the HIRES spectrograph ( $R = 48,000$ ) at Keck in 1998 when EX Lupi was at the maximum in a previous outburst. Herbig (2007) attributed the broad line emission to the accretion funnels, as the Fe II emission had inverse P Cyg profile with broad absorption longward at +300 km s<sup>-1</sup>. The velocity widths of the broad and the narrow components are 140 km s<sup>-1</sup> and 23 km s<sup>-1</sup> in Fe II 5018 Å, similar to the CO lines at 4.7  $\mu\text{m}$ . We looked for similar systematic redward absorption in the CO lines, and found that they are present in either epoch of the observations. Moreover, as we discuss later, the line profile in the outburst is double-peaked, which implies that the emitting gas is orbiting around the star. We conclude that the origin of the broad CO emission is not the stellar photosphere or accretion columns, but the circumstellar disk. We will deconvolve the broad and the narrow emission components using a simple slab model in the next sections.

### 3.2. Population Diagrams

First, population diagrams were constructed to obtain an overview of the physical property of the hot emitting gas in the disk. Equivalent widths of the emission lines were measured integrating  $v=1-0$   $P$ -branch lines over  $\pm 120$  km s<sup>-1</sup>. They thus include  $v=1-0$  emission of both broad and narrow components without correcting for the overlapping higher vibrational transitions. The column density at each rotational level is calculated as  $h\nu N_J A_\nu \cdot \pi R_s^2 = 4\pi d^2 W_\nu f_0$  from the equivalent widths  $W_\nu$ .  $f_0$  is the continuum flux coming from the  $M$ -band photometry. The specific radius of the emitting area  $R_s$  is set to 0.2 AU, so that it is roughly consistent with the line width of the broad line emission. The column density normalized by the degeneracy of the levels  $N_J/(2J+1)$  is plotted against the energy levels  $E_J/k$  in Fig. 4. The observed population diagrams show

turnovers at  $E_J/k = 3200\text{--}3400$  K, which testifies the emitting gas is optically thick. The vertical offset of the diagrams over 6 epochs spanned roughly an order of magnitude. The population diagram was initially fit by a thermodynamical model with  $T_x$  and  $N_{\text{CO}}$  as free parameters. However, in order to reproduce the sequences of  $N_J$  in the optical thick regime with an order of magnitude dispersion,  $N_{\text{CO}}$  has to be adjusted by several orders of magnitude up to  $10^{25}$  cm<sup>-2</sup>, which is apparently overstretching the capability of the model. We therefore fixed the column density to the minimum value of 6 epochs ( $N_{\text{CO}} = 2 \times 10^{20}$  cm<sup>-2</sup>) found in the first path of the fitting, and tried to match the absolute levels of  $N_J$  by changing the size of the emitting area. The column density  $2 \times 10^{20}$  cm<sup>-2</sup> is close to the upper limit of the physically feasible value of the relatively small area of the disk ( $R_s \sim 0.1$  AU,  $H/R=0.1$ ,  $[C/H]=10^{-4}$ ,  $n_{\text{H}} = 10^{12}$  cm<sup>-3</sup>). The fractional column density at  $v=1$  level was calculated with the vibrational temperature  $T_v$  set equal to  $T_x$ . The best-fit  $T_x$  is constrained within 1100–2400 K and tabulated in Table 3 with the corresponding emitting radii of the disk  $R_s$ . The line profile is assumed to be a Gaussian function of  $\sigma_v = 5$  km s<sup>-1</sup>.

### 3.3. Slab Model

Second, we used a simple slab model to incorporate the geometry and the rotation of the disk to reproduce the observed spectra. The slab model is a gas disk with no geometrical thickness, and meant to reproduce the underlying broad line emission only. The fundamental transition of CO is used as the sole opacity source at the wavelength concerned. No isotopomers are included, as this does not change the quality of the fit within the given signal-to-noise ratio of the spectra. Rotational levels up to  $J = 100$ , and vibrational levels up to  $v=8$  are taken into account. The wavelengths, energy levels, and Einstein  $A_\nu$  coefficients are taken from Goorvitch (1994). Ro-vibrational levels are populated according to the single-temperature Boltzmann distribution. Thermal broadening at the rotational temperature is taken as the only source of the intrinsic line width. The input parameters of thermodynamics, the total column density  $N_{\text{CO}}$ , and the rotational and vibrational temperatures  $T_x$  and  $T_v$ , are kept constant without radial dependency. The resulting spectrum is calculated as  $I_\nu = \frac{1}{4\pi} S_\nu (1 - e^{-\tau_\nu})$ , where  $S_\nu$  is the line source function  $A_{21}n_2/(B_{12}n_1 - B_{21}n_2)$ , and

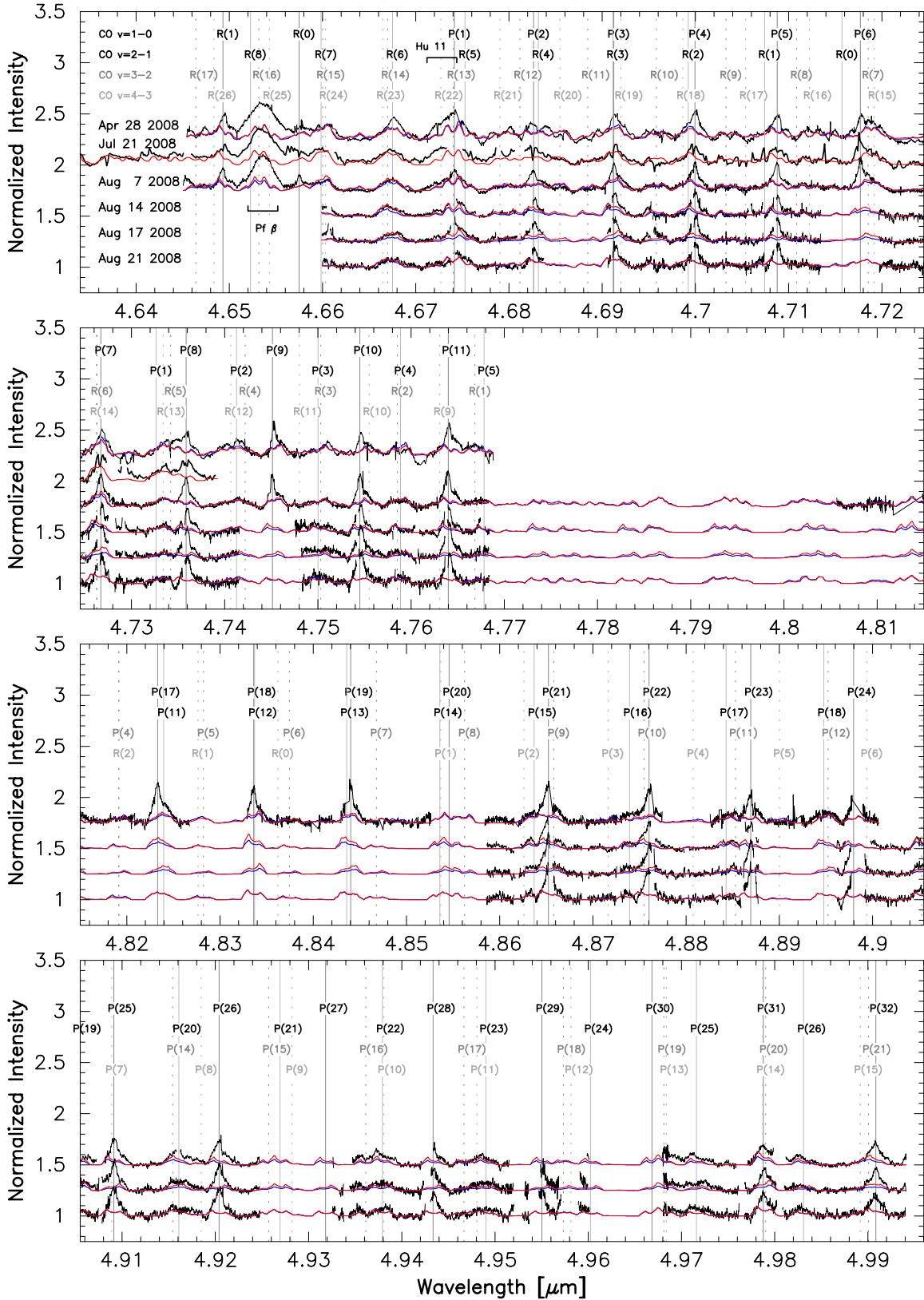


FIG. 2.— Spectra of EX Lupi at the CO fundamental band over six epochs from 28 April to 21 August 2008. All spectra were obtained by CRIRES at the *VLT* ( $R=100,000$ ) except on 21 July, when IRCS at Subaru Telescope was used with 5 times lower spectral resolution ( $R=20,000$ ). The spectra are normalized to the continuum level. Two emission components are immediately noticeable: one broad emission that fades away in August, and narrow line emission. Two model spectra for the outburst component are shown overlaid. The blue models are calculated with the excitation temperatures that fit the population diagrams in Fig. 4 and the constant column densities  $2 \times 10^{20} \text{ cm}^{-2}$ . The red models are calculated by fixing the excitation temperature at  $T_x = 4500 \text{ K}$ , which is the dissociation limit of the molecules. The two models supposedly represent the extreme cases meant to illustrate how the thermodynamical parameters are degenerated. The model parameters are listed in Table 3. The spectra are not covered continuously because of the gaps between the detector chips in CRIRES.

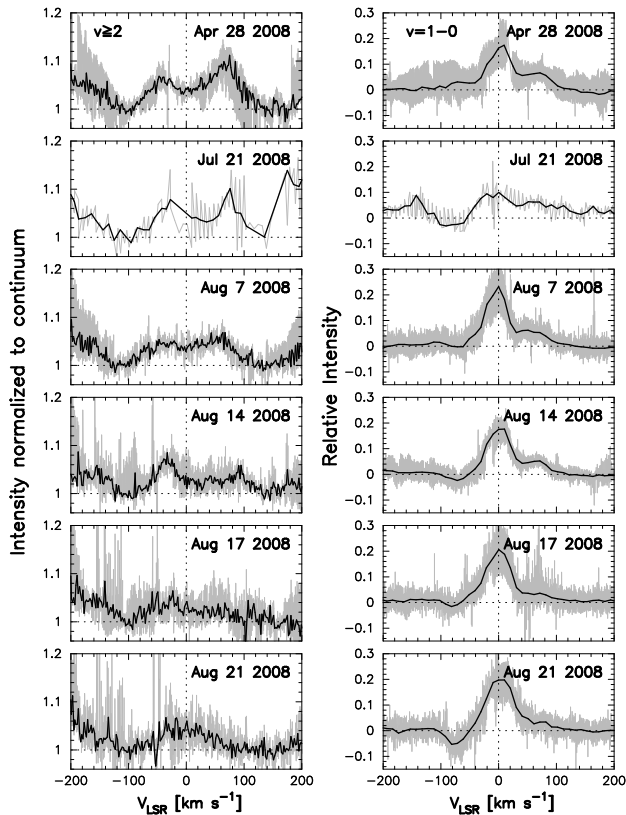


FIG. 3.— Left: composite line profiles of the vibrationally excited transitions ( $v \geq 2$ ). The gray lines are the overlay of CO  $P(3)$   $v=2-1$   $4.750 \mu\text{m}$ , CO  $P(4)$   $v=2-1$   $4.759 \mu\text{m}$ ,  $R(9)$   $v=3-2$   $4.703 \mu\text{m}$ , and  $R(21)$   $v=4-3$   $4.679 \mu\text{m}$ . The black line is the averaged spectrum. The line emission is double-peaked. Right: composite line profiles of CO  $v=1-0$  after the outburst models of  $T_x = 4500$  K in Figure 2 are subtracted. The gray lines are overlay of  $v=1-0$  lines within the spectral coverage, and the black lines are the averaged spectrum of them. A blue depression shows up at the velocity of  $-80 \text{ km s}^{-1}$  in August, and becomes deeper later. We attribute it to the disk wind started at the late phase of the outburst.

$\tau_\nu = \frac{h\nu_{12}}{4\pi} (n_1 B_{12} - n_2 B_{21}) \phi_\nu / \cos i$  is the opacity with  $\phi_\nu$  being the dimensionless line profile, and  $i$  being the disk inclination angle.

We tested a model with the opacity of the dust grains uniformly mixed with the gas. If we take the mass absorption coefficient  $\kappa(\lambda = 5 \mu\text{m}) = 2000 \text{ cm}^2 \text{ g}^{-1}$ , as calculated by Ossenkopf & Henning (1994), the line emission of CO will be entirely suppressed by the dust continuum emission, unless the gas to dust mass ratio is larger than 10,000. We infer that the continuum emission at  $5 \mu\text{m}$  comes from the region outside the broad line emission region. The continuum emission is therefore removed from the observed spectra, and only the remaining line emission part is produced by the slab model, without dust continuum opacity in the radiation.

The disk is divided into annuli from the inner ( $R_i$ ) to the outer disk ( $R_o$ ) boundary in the way that  $\log r_{j+1} - \log r_j$  is constant. The ro-vibrational emission spectrum is calculated in a small segment of each annulus with the given rotational and vibrational temperatures. The line spectra are then shifted by the radial velocity of the Keplerian rotation at the given azimuthal location, and added together. The stellar mass is assumed to be  $M_* = 0.6 M_\odot$  (Gras-Velázquez & Ray 2005). The line

emission spectra at the different radii are combined with an arbitrary weighting function  $I(r) = I(R_i) \left(\frac{r}{R_i}\right)^{-\alpha}$ , where  $\alpha$  is fixed to 2.5 in the present modeling. The inclination angles between  $40^\circ$  and  $50^\circ$  give reasonably good fits to the spectra at all the epochs. We therefore fixed it to  $i = 45^\circ$  without further adjustment. The disk model of Sipos et al. (2009), which reproduces the optical-infrared SED of EX Lupi in the quiescent phase favors face-on geometry with the most plausible inclination angle being  $i = 20^\circ$ . Sipos et al. (2009) found, however, that changing the inclination angle from  $0^\circ$  to  $40^\circ$  changes the output SED little; as the SED is relatively insensitive to the inclination angle, unless the disk is heavily optically thick. The inclination angle we adopt here is near the upper limit of this range.

## 4. DISCUSSION

### 4.1. Spectral Components

#### 4.1.1. Broad Line Emission

The disk parameters of the broad line emission that we modeled in the previous section,  $i$ ,  $R_i$ ,  $N_{\text{CO}}$ ,  $T_x$  and  $T_v$  are not independent, but interlocked in a non-trivial way. The line width of  $v \sin i \sim 150 \text{ km s}^{-1}$  on Apr 28 testifies that the radius of the inner edge of the disk is not larger than  $0.09 \text{ AU}$ . On the other hand, the disk cannot be too small in order to account for the absolute line flux. In the cases when the line profile is not simple and the signal-to-noise ratio is not high, such as the present case, the photometric calibration is important because the absolute line flux effectively constrains the size of the emitting region and therefore the disk radius. If we take the photometry at  $5 \mu\text{m}$  derived based on the spectroscopic data as face value, the single line flux ranges from  $10^{-14}$  to  $10^{-13} \text{ erg cm}^{-2}$ . The maximum flux density that we could retrieve from a disk at  $d$  pc away is  $f_\nu \approx \pi r^2 B_\nu(T_b) / d^2$ , where  $B_\nu$  is the Planck function. Given the blackbody temperature of  $T_b = 2000 \text{ K}$ , the distance of  $d = 155 \text{ pc}$ , and the line width of  $100 \text{ km s}^{-1}$ , we will get  $f_\nu < 10^{-14} \text{ erg s}^{-1} \text{ cm}^{-2}$ , if we assume a disk radius of  $0.01 \text{ AU}$ . This is too small to account for the observed line flux, therefore the radius of the inner hot disk cannot be smaller. The lower limit for the disk radius then calls for the inclination angle to be larger than  $i > 30^\circ$  to match the observed line width.

We first applied  $T_x$  and  $N_{\text{CO}}$  to the models as determined by the optically thick population diagrams, and optimized gas radius to fit the line profiles best. The vibrational temperatures  $T_v$  are set equal to  $T_x$ . The results underestimate the absolute line flux, because the outer radius  $R_o$  that is consistent with the kinematics in the line profiles is larger than the specific emitting radius  $R_s$  we used to reproduce the population diagrams. The model spectra are normalized by the square of  $R_o/R_s$  and shown in Fig. 2 in blue lines. The absolute line flux is reproduced without such an arbitrary scaling, by increasing the excitation temperature, allowing it to differ from  $T_v$ . However, when the emitting gas is hotter than  $3000 \text{ K}$ , the line ratios of different rotational transitions diminish in a short wavelength interval. It becomes less straightforward to determine  $T_x$  uniquely. In the optically thick regime, increasing  $N_{\text{CO}}$  and  $T_x$  imposes similar effects on the output spectra. In order to cope with the degeneracy, and avoid increasing the optical depth

TABLE 3  
DISK PARAMETERS FROM OUR MODELING.

Epoch	$R'_s$ <sup>a</sup> [AU]	$N'_{\text{CO}}$ <sup>b</sup> [ $\times 10^{19} \text{cm}^{-2}$ ]	$T'_x$ <sup>c</sup> [K]	$i$ <sup>d</sup> [ $^\circ$ ]	$R_o$ <sup>e</sup> [AU]	$R_o$ <sup>f</sup> [AU]	$\alpha$ <sup>g</sup>	$N_{\text{CO}}$ <sup>h</sup> [ $\times 10^{19} \text{cm}^{-2}$ ]	$T_v$ <sup>i</sup> [K]	$T_x$ <sup>j</sup> [K]	$a$ <sup>k</sup>	$F_\lambda$ <sup>1</sup> [ $\times 10^{-13} \text{W m}^{-2} \mu\text{m}^{-1}$ ]
28 Apr 2008	0.5	20	2100	45	0.05	0.3	2.5	6	3000	4500	0.7	5.9
21 Jul 2008	0.3	20	2400	45	0.05	0.3	2.5	4	2500	4500	1.0	3.4
7 Aug 2008	0.4	20	2200	45	0.055	0.4	2.5	2	2700	4500	0.8	4.5
14 Aug 2008	0.4	20	1300	45	0.05	0.3	2.5	1.5	2000	4500	-0.6	1.7
17 Aug 2008	0.5	20	1100	45	0.04	0.3	2.5	4	1800	4500	0.6	1.3
21 Aug 2008	0.4	20	1200	45	0.04	0.2	2.5	2	2000	4500	-0.8	1.2

<sup>a</sup> Radius of the emitting area from the population diagram in Fig. 4.

<sup>b</sup> Total column density of CO fixed to  $2 \times 10^{19} \text{cm}^{-2}$ .

<sup>c</sup> Rotational excitation temperature from the population diagram in Fig. 4.

<sup>d</sup> Inclination angle from face-on.

<sup>e</sup> Inner radius.

<sup>f</sup> Outer radius.

<sup>g</sup> Weight function of the intensity at different radius  $I(r) = I(R_i) (\frac{r}{R_i})^{-\alpha}$ .

<sup>h</sup> Total column density of CO.

<sup>i</sup> Vibrational excitation temperature.

<sup>j</sup> Rotational excitation temperature, fixed to 4500 K.

<sup>k</sup> Asymmetry factor of line profile.

<sup>1</sup> Flux density at the continuum level.

any further, which our simple model cannot handle, the rotational temperature was set to 4500 K, as the thermal dissociation temperature of CO is 4500–4600 K (Tatum 1966).  $T_v$  is adjusted so that the model reproduce the absolute line flux under the condition of  $T_x = 4500$  K. The second model with  $T_x = 4500$  K is shown in Fig. 2 in red lines. The two solutions (Table 3) can be regarded as the two extreme cases of the spectral models, and provide a fair idea how the model is affected by the degeneracy of the parameters. The best-fit line profile of a disk in Keplerian rotation sets the inner and the outer radius at 0.04–0.05 AU ( $=5$ – $7 R_*$ ) and 0.2–0.4 AU, respectively, for all epochs with the fixed inclination angle of  $i = 45^\circ$ . These geometric parameters are commonly used in the two representative models discussed above, and less subjected to the degeneracy. The optical depth is  $\tau_\nu = 0$ –1000 at the line center in the model with  $T_x = T_v$ , and  $\tau_\nu = 0$ –100 for  $T_x = 4500$  K, assuming the line is only thermal broadened.

Although the heavy overlap of the lines makes it difficult to discern the shape clearly, the line profile looks double-peaked (Fig. 3). This is the first time that the line profile is found to be double peaked in EXors. It lends support to the underlying similarity of the two classes of variable stars, FUors and EXors, and the origin of EXor outbursts associated with the circumstellar disk. Hartmann and his school (e.g. Hartmann & Kenyon 1996; Hartmann, Hinkle, & Calvet 2004; Zhu et al. 2009) attribute the split absorption lines of FUors, unusually broad for a stellar photosphere, to the gas in Keplerian rotation in unstable disks. The interval of line splitting is smaller in the near-infrared than in the visible. This is naturally explained if the absorption lines at longer wavelengths arise from the cooler, more distant, slow-rotating region (Zhu et al. 2009). On the other hand, Herbig, Petrov, & Duemmler (2003) and Petrov & Herbig (2008) found no correlation between the line widths and the excitation potentials of the visible absorption lines of FU Ori, which should be present if the lines arise from the disk, and the disk has a temperature gradient. They argued against the disk origin of the

optical lines, and claimed that the split lines are better reproduced by a large cool spot at the polar region on a rapidly rotating star. Moreover, the absorption lines of FUors are not perfectly Keplerian, but have a rectangular shape at the bottom (e.g. Hartmann, Hinkle, & Calvet 2004). It is hard to distinguish whether the unusual line shape represents the turbulence in the upper layer of the disk through which the absorption takes place, or a particular morphology and geometry of the cool spot on the surface of a star (e.g. Petrov & Herbig 2008). The line profile of EX Lupi is found to be double peaked, but in emission. The double peaked emission lines would not be compatible with the stellar spot hypothesis, unless the stellar surface is extended to at least a few times the stellar radius.

The line profiles are asymmetric between the blue and the red peaks. Figure 5 shows the blow-up view of the spectra near  $R(6) v=2-1$  ( $4.6675 \mu\text{m}$ ). There are minor contributions from  $R(14) v=3-2$  and  $R(23) v=4-3$  at  $4.6665 \mu\text{m}$  and  $4.6670 \mu\text{m}$ , respectively. The asymmetric line profile, however, cannot be fully explained by changing the vibrational temperature, thus the relative contribution of the three lines. The line profile is fitted better if we artificially introduce intrinsic asymmetry in the Keplerian line profile by modulating the azimuthal intensity distribution sinusoidally [ $I'_\nu(\theta) = I_\nu(\theta)(1 + (1-a) \cdot \sin \theta)$ , where  $a$  is the asymmetric factor] by down to  $a = 0.6$ . Asymmetries in infrared CO line emission have been found by Goto et al. (2006) in HD 141569 A, where the  $v=2-1$  emission is three times brighter in the northern disk than in the southern disk in the spatially resolved spectroscopy. Pontoppidan et al. (2008) proposed that the transition disks around SR 21 and HD 135344B have azimuthal structures, as the spectroastrometric signal of CO  $v=1-0$  is asymmetric, which is consistent with the millimeter dust continuum imaging (Brown et al. 2009). The line asymmetry of EX Lupi varies with time.

#### 4.1.2. Narrow Line Emission

The single peak profile of the narrow line emission with  $50 \text{ km s}^{-1}$  line-width in FWHM defies pure Keplerian rotation modeling, if the line intensity decreases as a power

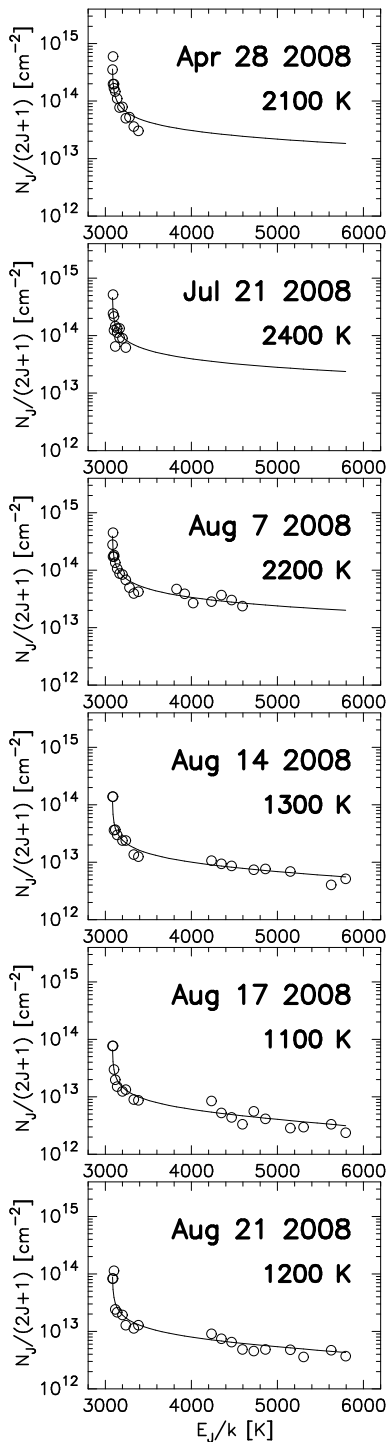


FIG. 4.— Population diagram of CO  $v=1-0$ . The line flux is calculated by integrating over  $\pm 120$  km  $s^{-1}$  of the emission lines. The emission is optically thick as is shown by the turnovers at  $E_J/k = 3000$ – $3400$  K. The thermodynamical models with assumed line profile (Gaussian profile with  $\sigma_v = 5$  km  $s^{-1}$ ) are shown overlaid.

law of the radius. Instead, the line width is simply taken as the orbital velocity of the gas, and is translated to the disk radius of 0.4 AU, using the same inclination angle as the broad line emission. FWHM was used instead of FWZI, as the latter is hard to measure unambiguously because of the overlap with the broad line components.

The disk radius above does not mean the inner truncation, but a characteristic radius where the narrow line emission arise from. The quiescent line emission comes exclusively from the  $v=1-0$  transition with no obvious higher vibrational transitions. Except the emergence of absorption at the blue shoulder implying a disk wind, no significant changes are found either in the equivalent width or in the line shape (Fig. 6; Fig. 3, right). Note that the small equivalent width on July 21 is of less significance than other epochs, as the data suffer from the low spectral resolution and the limited signal-to-noise ratio, which makes the removal of the telluric CO absorption challenging. The systematic error brought in by the telluric correction is magnified by the subtraction of the outburst model. The broad line emission is less subject to such problems in the measurements of the equivalent widths. The equivalent width of the narrow line component looks constant in time.

#### 4.1.3. Disk Wind

The model spectra of the broad line emission systematically overestimate the flux of  $v=1-0$  lines in the blue shoulder, and underestimate the red. After subtracting the spectral model, therefore, the  $v=1-0$  lines systematically show a blue depression between  $-40$  and  $-100$  km  $s^{-1}$  with excess emission at the red shoulder at  $+80$  km  $s^{-1}$ , which is similar to a P Cyg profile overlaid on the sharp quiescent emission (Fig. 3, right). This blueshifted absorption is more prominent toward the later epoch. The absorption lines can be noted at  $P(21)$  to  $P(26)$  on August 21, implying that the absorbing cloud is warm ( $T_x \gg 100$  K). The absorption is not likely photospheric, although EX Lupi is an M-type star in its quiescence, as the amount of blueshift is too large. The emergence of blue shifted absorption is also observed in infrared CO spectra of V1647 Ori toward the end of an outburst (Brittain et al. 2007). We infer that the blue absorption in the EX Lupi spectra also represents the disk wind, similarly to the case of V1647 Ori.

#### 4.2. Heating Mechanism

The excitation mechanism of the CO vibrational band is somewhat ambiguous. The elevated accretion energy can be directly converted to the kinetic energy of the gas through the viscous heating. In this case, the broad line emission that we locate at 0.04–0.4 AU traces the region where the accretion rate is high. On the other hand, the connection between the CO emission and the outburst could be indirect. The radiation from the central star, either from the hot accretion funnels or the footprints of the magnetic field lines, is first raised by the high disk accretion. The gas in the disk is heated afterwards by the enhanced irradiation. The primary difference of the two mechanisms is the vertical structure of the temperature that the heating imposes. In the case that the gas is viscously heated by the accretion, the disk is hottest near the mid-plane, and gradually cools down toward the surface. The emergent spectrum should be in absorption, as is the case for FUors (Hartmann, Hinkle, & Calvet 2004). When the irradiative heating is dominant, the temperature gradient is inverse with emission lines from the upper layer of the disk surface (Calvet et al. 1991a).

The irradiative heating has a few advantages to account for the CO line emission of EX Lupi. First, most



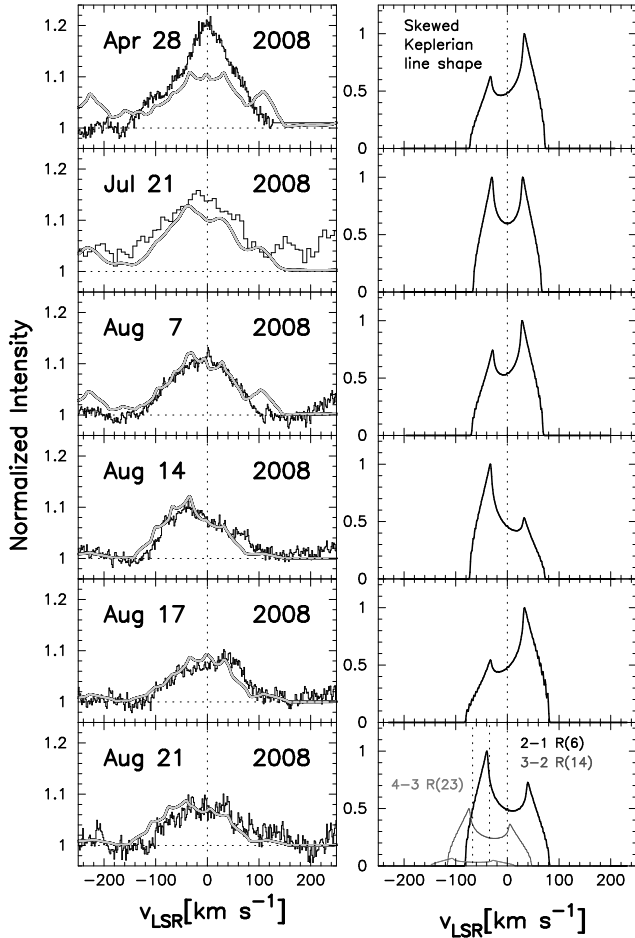


FIG. 5.— Line profile of the  $R(6)$   $v=2-1$  transition at  $4.6675 \mu\text{m}$ . The systemic velocity of EX Lupi is close to  $0 \text{ km s}^{-1}$  (Herbig, Petrov, & Duemmler 2003). The model spectra of the outburst with  $T_x = 4500 \text{ K}$  are overlaid in gray lines. There are minor contributions from the higher vibrational transitions of  $R(14)$   $v=3-2$  and  $R(23)$   $v=4-3$  as shown in the right bottom panel on 21 August. The observed line profiles cannot be reproduced without introducing the asymmetry. The asymmetry flips three times in August, which is consistent with the orbital period at  $0.04\text{--}0.06 \text{ AU}$ .

of the infrared CO emission lines observed today are thought to come from the hot surface of a disk, irradiatively heated (e.g. Najita et al. 2003). This is fully consistent with the line flux of the narrow line emission closely following the continuum level. A critical problem of the direct heating of gas by the accretion is the cooling time of the outburst. The duration of the EX Lupi outburst as is seen in the visible light curve, is roughly 8 months, from January to August 2008. The viscous time scale on which the gas accretes on the star is given by

$$\frac{1}{t_{\text{vis}}} = 3\pi \alpha (H/r)^2 \cdot \frac{1}{t_{\text{orbit}}},$$

for standard  $\alpha$  prescription of an accretion disk. The viscous time scale at  $0.04 \text{ AU}$  is 150 to 600 days, depending on  $H/r$  from  $0.05$  to  $0.025$  at the radius, even for the fastest case with  $\alpha$  being unity. The observed time scale of the outburst is uncomfortably short compared to the most optimistic case (Juhász et al. 2010).

On the other hand, some features of the EX Lupi out-

burst are not fully explained by the irradiative heating either. The line flux of both broad and narrow components decline with the visual magnitude and the continuum flux at  $5 \mu\text{m}$  (Fig. 6, upper panels), but on the slightly different decay rates. The narrow line emission is diminished by the factor of 4 from April to August (Table 4), which is the same factor with the decline of  $5 \mu\text{m}$  continuum flux, while the broad line emission is decreased faster by the factor of 10.

In order to contrast the decay rates, the equivalent widths are calculated in the same manner with the line flux. While the equivalent width of the narrow line emission maintains the level of  $1.5 \times 10^{-4} \mu\text{m}$  at the end of the outburst (Fig 6, bottom right), where the visible magnitude of EX Lupi returned to  $V = 12\text{--}13 \text{ mag}$ , comparable to the level of the pre-outburst brightness in 2007 (Fig. 1), the equivalent width of the broad line emission declines, keeping pace with the continuum flux at the visual wavelength. The differential time scale of the two line components is not accounted for, if the broad and the narrow line emissions are a single disk component radiatively heated in the identical manner.

In addition, the excitation state and the kinematics are distinct in two emission components, with no smooth transition between them. The characteristic radius where the narrow line emission arises from is  $0.4 \text{ AU}$ , and is constant as seen in the stable line width. The radius is immediately outside of the broad line emitting region at  $0.04\text{--}0.4 \text{ AU}$  (Fig. 7). The location of this transition zone is close to the inner-rim of the dust disk found by the SED modeling by Juhász et al. (2010). With the vibrational excitation state upto  $v=6$ , and the faster decay of the line flux than the radiatively heated narrow line component, the broad line emission apparently traces the outburst event more directly.

The heating mechanism of similar outburst variables, FUors, is most likely the elevated accretion near the disk-midplane, as the broad and double-peak CO lines in absorption testify (e.g. Hartmann, Hinkle, & Calvet 2004). To the contrary, the CO vibrational lines of EX Lupi are observed in emission in both overtone (Kóspál et al. 2010) and fundamental bands. The critical difference that might explain the emergent spectra of the two classes of the outburst variables is the optical depth of the disk. The broad line emitting region of EX Lupi is likely free of dust as is discussed above. The SED analysis by Juhász et al. (2010) also excludes the optically thick continuum emission either by gas or by dust grains within  $0.3 \text{ AU}$  during the outburst. Moreover, the accretion rate during the outburst is a few orders magnitude smaller in EX Lupi ( $\sim 10^{-7} M_{\odot} \text{ yr}^{-1}$ ) than FUors ( $\sim 10^{-4} M_{\odot} \text{ yr}^{-1}$ ), implying the lower disk surface density. The disk close to the midplane that is viscously heated by the accretion might be more exposed to the surface in the case of EX Lupi, which possibly makes the CO vibrational band observed in emission.

#### 4.3. Origin of Outburst

Let us extend our speculation to the trigger of the outburst, taking the physical scale of it being traced by the broad line emission. The physical size of the outburst on the scale of  $0.2\text{--}0.4 \text{ AU}$  argues against mechanisms that predict a global disk instability. Bonnell & Bastien (1992) proposed that a binary system can tidally disrupt

TABLE 4  
LINE FLUX AND EQUIVALENT WIDTH.

Epoch	JD	$F_{\lambda}(V)$ [ $\times 10^{-12} \text{ W m}^{-2} \mu\text{m}^{-1}$ ]	Line flux [ $\times 10^{-17} \text{ W m}^{-2}$ ]		Equivalent width [ $\times 10^{-4} \mu\text{m}$ ]	
			$v \geq 2^a$	$v=1-0^b$	$v \geq 2$	$v=1-0$
28 Apr 2008	2454585	4.5	$9.7 \pm 1.8$	$8.3 \pm 0.8$	$1.6 \pm 0.3$	$1.4 \pm 0.1$
21 Jul 2008	2454669	3.4	$4.9 \pm 2.5$	$2.7 \pm 0.6$	$1.4 \pm 0.7$	$0.8 \pm 0.2$
7 Aug 2008	2454686	1.6	$5.5 \pm 1.0$	$7.5 \pm 0.5$	$1.2 \pm 0.2$	$1.7 \pm 0.1$
14 Aug 2008	2454693	1.2	$1.7 \pm 0.5$	$2.3 \pm 0.2$	$1.0 \pm 0.3$	$1.4 \pm 0.1$
17 Aug 2008	2454696	0.4	$1.0 \pm 0.5$	$2.1 \pm 0.2$	$0.8 \pm 0.4$	$1.6 \pm 0.2$
21 Aug 2008	2454700	0.2	$0.9 \pm 0.4$	$2.2 \pm 0.2$	$0.7 \pm 0.3$	$1.7 \pm 0.1$

<sup>a</sup> Integrated over  $\pm 120 \text{ km s}^{-1}$ .

<sup>b</sup> Integrated over  $\pm 40 \text{ km s}^{-1}$ , after the spectral model with  $T_x = 4500 \text{ K}$  is subtracted.

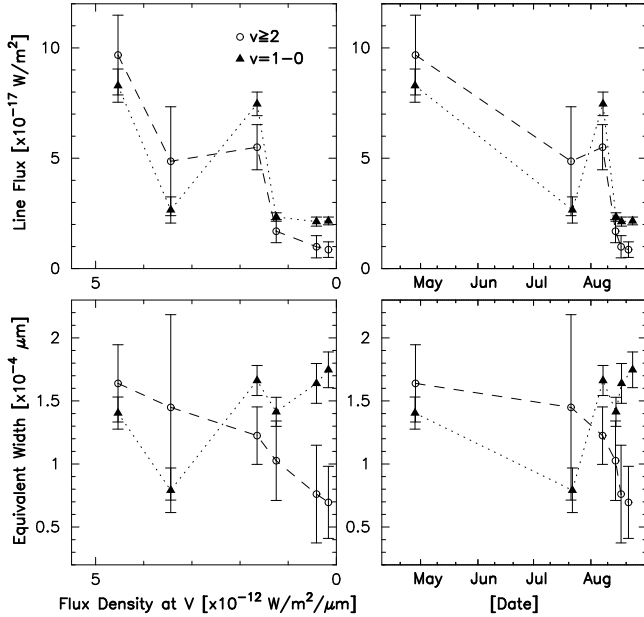


FIG. 6.— Top: (Left) Line flux of the emission lines from vibrationally excited states ( $v \geq 2$ , open circles), and the lowest transition  $v=1-0$  (triangles) after subtraction of the outburst model of  $T_x = 4500 \text{ K}$  shown as functions of the continuum flux of EX Lupi at the visible wavelength. The line intensity is integrated between  $-120$  and  $+120 \text{ km s}^{-1}$  for the broad line component. The composite line profiles used in the calculations are shown in Fig. 3. (Right) Same with the left panel, but shown with the date in abscissa. Bottom: Same with the top panels but for the equivalent widths. The line flux of the  $v \geq 2$  and  $v=1-0$  lines decrease with the time and the visual brightness of the star, but with different speed. The difference is clearly seen in the plots of the equivalent widths. The equivalent widths of the broader, highly excited lines decays quickly with the optical brightness of the star, while the equivalent widths of the  $v=1-0$  narrow line emission stays constant during the outburst.

the disks of each other in a close encounter, and temporarily increase the accretion rate up to  $10^{-4} M_{\odot} \text{ yr}^{-1}$ . The tidal disruption by a companion is attractive because it naturally explains the repetitive nature of EXor outbursts. The binary fraction among low-mass pre-main sequence stars is indeed high (e.g. Ghez et al. 1993). FU Ori, the prototype FUor, has a close companion (Wang et al. 2004), and there are even FUor-like binaries where both of the binary components are FUor-like, which is statistically unlikely if two are randomly paired (Reipurth & Aspin 2004). The gravitational disruption by a binary companion may work for the present case as a trigger of the disk instability combined with other

mechanisms, but most likely does not explain the small radius of the high mass-accretion region by itself. No visible (Ghez et al. 1997; Bailey 1998) or spectroscopic companion (Herbig 2007) to EX Lupi has been identified as of today.

Vorobyov & Basu (2006) argued that planetary cores – which possibly have already formed in a gravitationally unstable disk – can trigger an FUor outburst when they migrate inward and eventually fall into the central star. Protoplanetary clumps form at  $>10-50 \text{ AU}$  away from the star. The migration from the outer disk over this distance does not explain the discrete boundary at  $0.2-0.4 \text{ AU}$  either. Their simulation ends at the inner radius of  $0.5 \text{ AU}$ . Further investigation how the infalling a protoplanetary clump behaves in the final  $0.5 \text{ AU}$  is awaited.

When mass inflow from the outer disk is faster than what the inner disk can transport further in, the accretion slows down, and piles up material at the boundary between the inner and the outer disk. The elevated surface density triggers a local disk instability, and the accretion mode switches to a higher state. The mass accretion could slow down at a certain radius simply because the disk viscosity is too low, or the viscosity is locally too low because of the decoupling of the disk and the magnetic field, or if the disk has a gap, or if it is magnetically truncated.

The disk viscosity is provided by the coupling of the magnetic field and slightly ionized medium in the MHD instability model. Deep inside the disk where the stellar radiation no longer penetrates, there is a low ionization region called the dead zone, where the viscosity is close to zero. The incoming mass piles up there, until the surface density becomes high enough to heat the disk to  $\approx 1000 \text{ K}$  to restore the coupling with the magnetic field.

A dead zone starts at  $0.1 \text{ AU}$ , and extends beyond  $1 \text{ AU}$  in a disk around a solar mass star (Gammie 1996). The disk instability is triggered at the coldest region of the dead zone near the outer boundary (Armitage et al. 2001). Zhu et al. (2007) constructed a radiation transfer model of the disk around FU Ori in outburst, and calculated the size of the active region to be around  $1 \text{ AU}$ , which naturally fits with MHD disk instability. The observed transition region of EX Lupi is a few times smaller than the typical size of a dead zone. This may not be surprising, as the luminosity of EX Lupi in quiescence is small as well [ $L_* < 0.5 L_{\odot}$  in Gras-Velázquez & Ray (2005),  $L_* = 0.75 L_{\odot}$  in Sipos et al. (2009)].

Wünsch et al. (2005) discovered another type of insta-

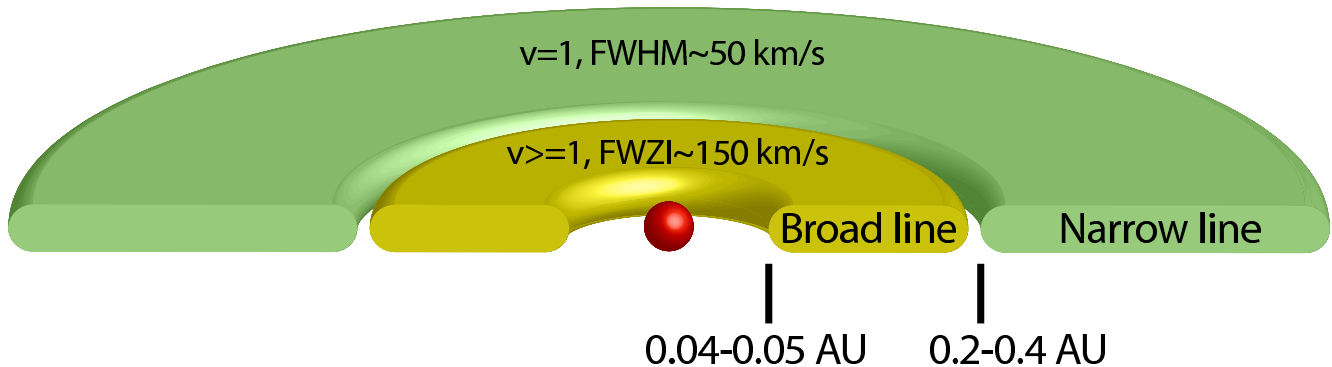


FIG. 7.— Schematic representation of the broad and the narrow line emitting regions discussed in the text.

bility near the inner edge of the dead zone in their numerical model. When a small perturbation is applied to the height of the dead zone, the mass inflow locally increases while the outgoing mass decreases. The height of the perturbed region grows, until it splits up from the dead zone and triggers a ring instability, or the inner edge of the dead zone starts oscillating radially (Wünsch et al. 2006). This instability works at the correct physical scale of 0.1–0.2 AU with small accretion rates  $10^{-9} M_{\odot} \text{ yr}^{-1}$  which are appropriate for EX Lupi. However, the predicted timescale of the outburst is 100 yrs or longer. This is close to the observed timescales of FUor outburst, but is too long for EX Lupi ( $\sim 1$  yr).

When a star is strongly magnetized, the gas infall stops at the radius where the Keplerian angular velocity is equal to the stellar rotation, as the orbital motion of the gas is tied to the star. The matter piles up at the corotation radius, until the surface density becomes so high that the thermal pressure of the gas overcomes the magnetic pressure (D’Angelo & Spruit 2010). This mechanism requires the presence of a strong magnetic field. Among young eruptive stars, FU Ori is the first where a magnetic field was discovered in its disk (Donati et al 2005). There are no attempts known to date, however, to measure the magnetic field of EX Lupi. The inner rim of the high accretion region we measured (0.04–0.05 AU) translates to a period of 4–5 days assuming Keplerian rotation. The typical rotation time for T Tauri stars is a few days to a week (e.g. Rodríguez-Ledesma et al. 2009). The rotation period of EX Lupi itself is however not known yet.

A self-regulated thermal instability theory assumes relatively high, constant inflow of mass ( $10^{-6} M_{\odot} \text{ yr}^{-1}$ – $10^{-7} M_{\odot} \text{ yr}^{-1}$ , Clarke et al. 1989; Bell & Lin 1994). The constant mass transportation is hindered at a certain radius, where the viscosity is simply too low to drain the incoming mass in time. The material piles up until the surface density becomes high enough to thermally ionize the gas. Near the ionization front, the disk opacity increases with temperature due to negative hydrogen ions adding continuum opacity (Faulkner, Lin, & Papaloizou 1983). Thermal instability is triggered by the runaway local heating of the disk. The transition front propagates outward until the instability is suppressed at the radius where the viscous heating is no longer effective to keep the disk warm. The radius at which the thermal instability is turned off is a function of the mass accretion.

It is 0.1 AU for a fiducial star of  $1 M_{\odot}$  with  $3 R_{\odot}$  with a constant mass accretion of  $3 \times 10^{-6} M_{\odot}$  (Bell & Lin 1994).

Self-regulating thermal instability is well studied in the parameter space suited to FUors. The mechanism seems to work with accretion rates from  $\dot{M} = 10^{-7} M_{\odot} \text{ yr}^{-1}$  to  $\dot{M} = 10^{-5} M_{\odot} \text{ yr}^{-1}$ , and is able to reproduce the observed flaring magnitude at optical wavelengths ( $\approx 5$  mag), the rise time to the maximum ( $\sim 1$  year), and the duration of the outburst (decades to a century). These physical parameters are one order of magnitude smaller in the case of EX Lupi, with the quiescent phase accretion rate being  $\dot{M} = 4 \times 10^{-10} M_{\odot} \text{ yr}^{-1}$  (Sipos et al. 2009), which goes up to  $\dot{M} = 2 \times 10^{-7} M_{\odot} \text{ yr}^{-1}$  in the outburst (Juhász et al. 2010) with the rise time of a month, and duration of about a year. It is yet to be seen if the self-regulating thermal instability works for the small accretion rate with no external triggers to cooperate.

An interesting possible triggering mechanism is an embedded planet. When a protoplanet opens a gap, the mass transportation stops at its outer edge. The mass is banked up until the thermal instability is triggered (Lodato & Clarke 2004; Clarke & Syer 1996). With the additional degrees of freedom of the mass of the planet and its location, this model could cover a wider parameter space, and closely reproduce the observed properties of FUor outbursts. The triggering via embedded planet makes the instability propagate initially outside in, and qualitatively reduces the rise time. The smaller the mass of the planet, the smaller the outburst, triggered by the smaller accretion rate. It is still to be seen though, if the mechanism works for EX Lupi, as the exact parameter space of EX Lupi outburst is not covered in the models by Lodato & Clarke (2004).

#### 4.4. Variation of Line Profile Asymmetry

Nevertheless, a possible planet in the disk is interesting in connection with the temporal variation of the line symmetry in CO emission spectra (Fig. 5). The line asymmetry indicates that the receding side of the disk was brighter on August 7, but by August 14 the approaching side became brighter. The receding part is again brighter 3 days later, which again moved to the other side in 4 days. The modulation of the line profile on the timescale of 3–4 days was known in the visible spectra of FU Ori and V1057 Cyg. Herbig, Petrov, & Duemmler (2003) discussed two possible origins of the variation, that the

modulation comes from the stellar spot and that it comes from the hot spot in the circumstellar disk, which may or may not be related to the hot accretion columns rising out of the disk. In the case of V1057 Cyg, the line modulation is not accompanied by photospheric variability, which makes the stellar spot hypothesis difficult. On the other hand, the line modulation in V1057 Cyg is stable over 3 yrs, which also makes the hot spot on a differentially rotating disk unlikely. The question of whether the hot spot resides on the photosphere or on the disk is therefore still open.

The period of the spectroscopic modulation of EX Lupi is hard to constrain with only six epochs of observations. If we simply take 7 and 3.5 days as half the period of the orbit in the first and the second half of August, the locations of the hot spot are 0.06 and 0.04 AU, respectively. This is within the span of the active disk that we derived from the outburst model, with the latter location close to the inner edge. Further spectroscopic monitoring with finer temporal sampling should be done in order to tell whether this represents real migration of a hot spot in the disk, as well as the theoretical study on the fate of protoplanetary clumps that fall into the star (Vorobyov & Basu 2006). A more general discussion on the line asymmetry caused by a planet embedded in the disk is found in Regály et al. (2010).

## 5. SUMMARY

Here is the summary of our results, and possible directions for future investigations.

- We reported the results of a spectroscopic monitoring campaign of EX Lupi in the CO vibrational fundamental band at 4.6–5.0  $\mu\text{m}$ . The observations covered six epochs in the outburst, which started in early 2008.
- We detected high temperature CO gas in the emission-line spectra, that apparently consist of two distinct components. The equivalent width of the broad line emission ( $\text{FWZI} \sim 150 \text{ km s}^{-1}$ ) decays with the visual brightness of the star. The gas is vibrationally hot with the highly excited lines detected up to  $v=6$ .
- The line profiles of the broad line component are double peaked, indicating that the gas is in a circumstellar disk. We used a simple slab model to locate the hot gas to the annulus 0.04–0.4 AU. There is strong asymmetry in the line profiles that varies with time on the order of days to week, implying the presence of a hot spot on the disk.
- There is a second component of the line emission near the systemic velocity of EX Lupi with much narrower line profiles ( $\text{FWHM} \approx 50 \text{ km s}^{-1}$ ). The

narrow line emission is vibrationally cool; it exclusively consists of  $v=1-0$  transitions. The line width indicates that the characteristic radius of the emitting gas is 0.4 AU, larger than the radius where the broad line emission arises. The equivalent widths of the narrow lines are constant over the whole observing period.

- An additional disk wind is found as absorption lines centered at  $-80 \text{ km s}^{-1}$  toward the end of the outburst. A similar disk wind was observed previously in V1647 Ori.
- The two emission components are distinct in the decay rate, the excitation state, and the kinematics. If the broad line emission traces the high accretion region, its compact size favors local disk instabilities where a disk goes through bimodal accretion. Major local disk instability theories, such as thermal instability, magnetohydrodynamical instability, magnetospheric truncation of a disk partially fit to the profile of the outburst, albeit our data did not allow to distinguish between these theories. The origin of the outburst involving global disk instabilities are unlikely.

Most of the disk instability theories today have been tested against FUor outbursts, but little theoretical work has been done for EXors. It is not clear at the moment if the missing proper model for EX Lupi outbursts is due to an intrinsic difficulty in reproducing such small and frequent outbursts with low accretion rate, or is due to a lack of exploration in the parameter space that fits to EXor outbursts. Our attempts to remedy this are also hindered by missing fundamental parameters of EX Lupi. The period of the stellar rotation and magnetism, as well as an accurate simultaneous photometric calibration of the spectra at the time of the observation would help to improve the modeling of the outburst.

We appreciate the anonymous referee for the constructive criticisms to improved the manuscript. We thank all the staff and crew of the *VLT* and Subaru for their valuable assistance in obtaining the data. M.G. thanks Takeshi Oka for patient enlightening of her in thermodynamics of CO. M.G. also thanks Bringfried Stecklum and Andreas Seifahrt for instructive discussion and encouragement to finish the paper. Zs.R. was partly supported by MÖB/DAAD-841 Mobility Grant. A.C. acknowledge support from a Swiss National Science Foundation grant (PP002-110504). P.Á. acknowledges support from the grant OTKA K62304 of the Hungarian Scientific Research Fund. The research of Á.K. is supported by the Netherlands Organization for Scientific Research. A.S.A. acknowledges support from the Deutsche Forschungsgemeinschaft (DFG) grant SI 1486/1-1. We appreciate the hospitality of Chilean and Hawaiian community that made the research presented here possible.

## REFERENCES

- Ábrahám, P., Juhász, A., Dullemond, C. P., Kóspál, Á., van Boekel, R., Bouwman, J., Henning, T., Moór, A., Mosoni, L., Sicilia-Aguilar, A., & Sipos, N. 2009, *Nature*, 459, 224
- Aikawa, Y., Nomura, H. 2006, *ApJ*, 642, 1152
- Armitage, P. J., Livio, M., & Pringle, J. E. 2001, *MNRAS*, 324, 705
- Aspin, C., Beck, T. L., & Reipurth, B. 2008, *AJ*, 135, 423
- Bailey, J. 1998, *MNRAS*, 301, 168

- Bell, K. R., & Lin, D. N. C. 1994, *ApJ*, 427, 987
- Bell, K., R., Lin, D. N. C., & Ruden, S. P. 1991, *ApJ*, 372, 633
- Bonnell, I., & Bastien, P. 1992, *ApJ*, 401, L31
- Bonnet et al. 2004, *The ESO Messenger*, 117, 17
- Brittain, S., Rettig, T. W., Simon, T., Balsara, D. S., Tilley, D., Gibb, E., & Hinkle, K. 2007, *ApJ*, 670, L29
- Brown, J. M., Blake, G. A., Qi, C., Dullemond, C. P., Wilner, D. J., & Williams, J. P. 2009, *ApJ*, 704, 496
- Calvet, N., Hartmann, L., & Kenyon S. J., 1991, *ApJ*, 383, 752
- Calvet, N., Patino, A., Magris, G. C., & D'Alessio, P. 1991, *ApJ*, 380, 617
- Clarke, C. J., Lin, D. N. C., & Papaloizou, J. C. B. 1989, *MNRAS*, 236, 495
- Clarke, C. J. & Syer, D. 1996, *MNRAS*, 278, L23
- D'Angelo, C. R., & Spruit, H. astro-ph/0011742
- Donati, J.-F., Paletou, F., Bouvier, J., & Ferreira, J. 2005, *Nature*, 438, 466
- Faulkner, J., Lin, D. N. C., & Papaloizou, J. 1983, *MNRAS*, 205, 359
- Fedele, D., van den Ancker, M. E., Petr-Gotzens, M. G., & Rafanelli, P. 2007, *A&A*, 472, 207
- Gammie, C. F. 1996, *ApJ*, 457, 355
- Ghez, A. M., McCarthy, D. W., & Patience, J. L. 1997, *ApJ*, 481, 378
- Ghez, A. M., Neugebauer, G., & Matthews, K. 1993, *AJ*, 106, 5
- Goorvitch, D., 1994, *ApJS*, 95, 535
- Goto, M., Usuda, T., Dullemond, C. P., Henning, Th., Linz, H., Stecklum, B., & Suto, H. 2006, *ApJ*, 652, 758
- Gras-Velázquez, Á., & Ray, T. P. 2005, *A&A*, 443, 541
- Greene, T. P., Aspin, C., & Reipurth, B. 2008, *ApJ*, 135, 1421
- Hartmann, L., & Kenyon, S. J. 1996, *ARA&A*, 34, 207
- Hartmann, L., Hinkle, K., & Calvet, N. 2004, *ApJ*, 609, 906
- Hayano, Y. et al SPIE, 2008, *Proc. SPIE*, 7015, 25
- Herbig, G. H. 1950, *PASP*, 62, 211
- Herbig, G. H., Aspin, C., Gilmore, A. C., Imhoff, C. L., & Jones, A. F. 2001, *PASP*, 113, 1547
- Herbig, G. H. 1989, *ESO Workshop on Low Mass Star Formation and Pre-Main Sequence Objects*, p. 233 - 246
- Herbig, G. H., Petrov, P. P., & Duemmler, R. 2003, *ApJ*, 595, 384
- Herbig, G. H. 2007, *AJ*, 133, 2679
- Herbig, G. H. 2008, *ApJ*, 135, 637
- Juhász, A., et al. 2010, in prep.
- Käuffl, H. U., et al. 2004, *Proc. SPIE*, 5492, 1218 .
- Koornneef, J. 1983, *A&A*, 128, 84
- Kóspál, Á. et al. 2010, in prep.
- Lodato, G., & Clarke, C. J. 2004, *MNRAS*, 353, 841
- Lombardi, M., Lada, C. J., & Alves, J. 2008, *A&A*, 480, 785
- Lord, S. D. 1992, *A New Software Tool for Computing Earth's Atmosphere Transmissions of Near- and Far-Infrared Radiation*, NASA Technical Memoir 103957 (Moffett Field, CA: NASA Ames Research Center)
- Najita, J., Carr, J. S., Glassgold, A. E., Shu, F. H., & Tokunaga, A. T. 1996, *ApJ*, 462, 919
- Najita, J., Carr, J. S., & Mathieu, R. D. 2003, *ApJ*, 589, 931
- Ossenkopf, V., & Henning, Th. 1994, *A&A*, 291, 943
- Reipurth, B., & Aspin, C. 2004, *ApJ*, 608, L65
- Rettig, T. W., Haywood, J., Simon, Th., Brittain, S. D., & Gibb, E. 2004, *ApJ*, 616, L163
- Regály, Zs. et al. in press.
- Rodríguez-Ledesma, M. V., Mundt, R. & Eisloffel, J. 2009, *A&A*, 502, 883
- Petrov, P. P., & Herbig, G. H. 2008, *AJ*, 136, 676
- Pontoppidan, K. M., Blake, G. A., van Dishoeck, E. F., Smette, A., Ireland, M. J., & Brown, J. 2008 *ApJ*, 684, 1323
- Sicilia-Aguilar, A. et al. 2010, in prep.
- Sipos, N., Ábrahám, P., Acosta-Pulido, J., Juhász, A., Kóspál, Á., Kun, M., Moór, A., & Setiawan, J. 2009, *A&A*, 507, 881
- Tatum, J. B., 1966, *Publ. Dom. Astrophys. Obs. Victoria*, 13, 1
- Tokunaga, A. T., et al. 1998, *Proc. SPIE*, 3354, 512
- Infrared Astronomy*, in Chapter 7 pp.143-164, 'Allen's Astrophysical Quantities Fourth Edition' ed. A. N. Cox Springer-Verlag, New York, Berlin, Heidelberg
- Vorobyov E. I., & Basu, S. 2006, *ApJ*, 650, 956
- Wang, H., Apai, D., Th. Henning, & Pascucci, I. 2004, *ApJ*, 601, L83
- Wünsch, R., Gawryszczak, A., Klahr, H., Róžyczka, M. 2006, *MNRAS*, 367, 773
- Wünsch, R., Klahr, H., Róžyczka, M. 2005, *MNRAS*, 362, 361
- Zhu, Zhaohuan, Espaillat, C., Hinkle, K., Hernandez, J., Hartmann, L., & Calvet, N., 2009, *ApJ*, 694, L64
- Zhu, Zhaohuan, Hartmann, L., Calvet, N., Hernandez, J., Muzerolle, J., & Tannirkulam, A.-K. 2007, *ApJ*, 669, 483